

# Full Dimensional Quantum Calculations of Vibrational Energies of *N*-Methyl Acetamide

A. L. Kaledin\* and J. M. Bowman

Department of Chemistry and Cherry L. Emerson Center for Scientific Computation, Emory University, Atlanta, Georgia 30322

Received: March 26, 2007; In Final Form: May 2, 2007

We report quantum calculations of vibrational states of trans *N*-methyl acetamide ( $\text{H}_3\text{C}-\text{HNCO}-\text{CH}_3$ ) in full dimensionality using the code MULTIMODE. In this code, the full potential is represented as a hierarchical sum of  $n$ -mode potentials in the normal coordinates. All 30 one- and 435 two-mode potentials are included in the sum, as well as a restricted set of 10 three-mode potentials corresponding to the experimentally probed amide band. The electronic energies on the various  $n$ -mode grids are obtained using ab initio Møller–Plesset perturbation theory with a triple- $\zeta$  quality, correlation-consistent basis set. Convergence tests of the low-lying vibrational eigenvalues of the amide band show that this limited three-mode representation of the full potential yields well converged results that are in excellent agreement with experiment. The infrared spectrum in the region of the amide bands is calculated and also agrees well with experiment.

## 1. Introduction

Spectroscopic investigation of *N*-methyl acetamide (NMA), which is considered a model for a peptide bond in proteins, can provide information about secondary structure of proteins in the gas phase as well as in solution. Numerous infrared (IR) and Raman experiments have focused on the spectral region spanned by the three amide bands of NMA,<sup>1–8</sup> particularly in the easily detectable amide I regime that overlaps with the CO stretch. In liquid water, the CO stretch responds to the presence of water molecules by forming hydrogen bonds, and the resulting frequency shift can be used to assess the dynamics of protein–solvent interactions. Similarly, the amide II and amide III bands, which overlap with the NH in-plane wagging motion, can be used to describe the interaction between CO and HN, which are part of the backbone of a protein. And since the amide hydrogen can form a bond with the solvent, that is,  $\text{H}_2\text{O}\cdots\text{H}-\text{N}$ , corresponding frequency shifts provide further information on protein behavior in aqueous solution.

Recent high-level theoretical studies<sup>4,9,10</sup> have added new insight to the simplified, harmonic, or empirical force-field-based models. Vibrational calculations that go beyond the harmonic model were reported recently by Gregurick et al.<sup>10</sup> This group performed 28 080 electronic energy calculations using Møller–Plesset perturbation theory (MP2) and a double- $\zeta$ -plus-polarization (DZP) basis set on all one- and two-mode grids in normal coordinates. The vibrational analysis was performed using the vibrational self-consistent field (VSCF) method with an MP2 treatment of mode–mode correlation. A major goal of that work was to compare the ab initio-based results and those using an empirical force field from AMBER<sup>11</sup> with experimental energies from rare-gas matrix data. Although the two sets of vibrational calculations were roughly at the same level of agreement with experiment, the authors argued that the ab initio approach was superior to the empirical force field. The “ab initio” approach showed differences of 18–43  $\text{cm}^{-1}$  with experiment for the three amide bands and even larger differences with experiment for other bands.

Theoretical studies of the effect of solvation on the amide bands have also been undertaken. Ab initio molecular dynamics simulations of *N*-methyl acetamide have been carried out in gas phase and explicit solvent.<sup>12–15</sup> Several groups, including Gaigeot et al.<sup>13</sup> and Mantz et al.,<sup>14</sup> have used Car–Parrinello density functional (CP/DFT) molecular dynamics<sup>16</sup> to study solvation effects and infrared spectroscopy of the amide bands. The simulated spectra had the correct qualitative shapes, as compared to the experiment; however, the positions of some of the dominant peaks, for example, the CO stretch, were found to be off from the experiment by up to 100  $\text{cm}^{-1}$ .<sup>13</sup> These discrepancies are likely due to the small electron basis sets, for example, a nonpolarized double- $\zeta$  quality valence basis set, used in these CP/DFT calculations. These calculations may describe well the geometry of the complex but fail to produce the correct curvature of the potential surface, even in the vicinity of the minimum.

An interesting step to improve the ab initio treatment of the amide modes and also to account for solvent effects was taken by Hayashi et al.<sup>15</sup> They developed a DFT-based force field for the five modes, including the three amide modes, plus two other “A” modes that have frequencies within the amide band spectral region. They modeled the effect of water by performing extensive MD runs in a periodic box using a force field. The electrostatic field due to the water molecules was fitted to a polynomial in the Cartesian coordinates of NMA. The potential energy of NMA in the presence of the solvent was then recreated via a fifth-order Taylor series with the expansion coefficients as parameters of the electric field. These electronic structure calculations were done at the level of DFT. The calculated gas-phase frequencies for the entire amide band matched the experiment very well, and the predicted red shift of amide I due to solvation in water came out very close to the measured value. It is important to stress that such good agreement was achieved despite the reduced dimensionality treatment of the system; to note, only the five in-plane vibrational modes, spanning the entire amide band region, were treated explicitly in the quantum dynamical calculation.

In this paper, we report a full dimensional ab initio approach to the vibrational energies of NMA and the IR spectrum in the

\* Corresponding author. E-mail akaledi@emory.edu.

region of the amide bands that goes beyond what was reported previously both in terms of the level of ab initio treatment of the electronic energies and the level of mode coupling. Clearly, a straightforward, full-dimensional (30 degree-of-freedom), global potential energy surface for NMA is not a realistic goal at present. We take a different approach, which nevertheless allows us to perform vibrational calculations in full dimensionality, using MULTIMODE.<sup>17</sup> The key aspect of this approach is the  $n$ -mode representation of the potential,<sup>18,19</sup> which permits a “direct” evaluation of the ab initio electronic energies on  $n$ -mode grids. With these potential grids in hand, MULTIMODE then calculates vibrational eigenvalues and eigenfunctions of the exact vibrational Hamiltonian given by Watson.<sup>20</sup> We describe this approach in the next section, and in Section 3, we present our results and comparison with experiment. A summary and directions for future research are given in Section 4.

## 2. Evaluation and Fitting of the NMA Potential

The vibrational approach taking in the code MULTIMODE is based on normal mode coordinates. In the case of NMA, there are 30 normal modes, and in principle, the potential depends on all of these coordinates. An approach to deal with this very high dimensionality is to use a hierarchical  $n$ -mode representation ( $n$  MR) of the potential. In normal coordinates, this is given by<sup>18</sup>

$$V = \sum_i V^{(1)}(Q_i) + \sum_{i < j} v^{(2)}(Q_i, Q_j) + \sum_{i < j < k} v^{(3)}(Q_i, Q_j, Q_k) + \dots \quad (1)$$

where  $V^{(1)}(Q_i)$  is the one-mode potential energy along displacement  $Q_i$ , while  $Q_{j \neq i} = 0$  for all  $j$ . This necessarily implies that the heretofore defined intrinsic potential  $v^{(2)}(Q_i, Q_{j \neq i})$  is coupling between modes  $i$  and  $j$ , which vanishes when  $Q_i = 0$  or  $Q_j = 0$ , that is,  $v^{(2)}(0, Q_j) = v^{(2)}(Q_i, 0)$ . In general,  $v^{(m)}(\dots, 0, \dots) = 0$  is true for any intrinsic potential. Thus, an intrinsic two-mode potential is defined as  $v^{(2)}(Q_i, Q_j) = V^{(2)}(Q_i, Q_j) - V^{(1)}(Q_i) - V^{(1)}(Q_j)$ , where  $V^{(2)}(Q_i, Q_j)$  is the full two-mode potential. Similarly, a three-mode intrinsic potential is defined as  $v^{(3)}(Q_i, Q_j, Q_k) = V^{(3)}(Q_i, Q_j, Q_k) - v^{(2)}(Q_i, Q_j) - v^{(2)}(Q_i, Q_k) - v^{(2)}(Q_j, Q_k) - V^{(1)}(Q_i) - V^{(1)}(Q_j) - V^{(1)}(Q_k)$ , and so on.

This representation of the potential has been shown to yield essentially exact vibrational energies in full-dimensionality for semirigid molecules, with  $n$  significantly less than the total number of vibrational modes. A recent example is for nine-mode  $\text{CH}_4$ ,<sup>19,21–23</sup> in which a 5-mode representation of the potential was sufficient to yield energies to within several tenths of a wave number for all states 4600  $\text{cm}^{-1}$  above the zero-point energy. Another very relevant advantage of the  $n$ -mode representation of the potential is that a “direct” calculation of ab initio energies on the relevant  $n$ -mode grids for the intrinsic potentials is all that is needed to implement a calculation. This technique using at least three-mode coupling has been performed by us,<sup>24</sup> Yagi et al.,<sup>25</sup> and Rauhut<sup>26</sup> with and without interpolation. Gerber and co-workers have done extensive similar calculations using direct calculations on two-mode grids.<sup>27</sup> The latter group used this approach to calculate the fundamental transition frequencies of NMA at a 2MR level of theory, as discussed above.<sup>10</sup>

In the present application to NMA, this direct approach is clearly necessary; however, to go beyond the two-mode approach of Gregurick et al.,<sup>10</sup> by treating all 30 modes at the same level of  $n$ -mode coupling would not be feasible. Specifically, there are 435 two-mode intrinsic potentials and 4060

three-mode intrinsic potentials. So clearly, even if effective interpolation can be performed on grids for these potentials such that, say, 125 points are sufficient for each three-mode potential, that would still amount to 507 500 ab initio energies. Obviously, this would not be a feasible calculation. In response to this, we have modified MULTIMODE to allow for a flexible choice of modes to describe different levels of mode coupling among different groups of modes. In the present case, we treat the five amide modes (described in detail in the next section) up to three-mode coupling and the remaining 25 modes up to two-mode coupling. This reduces the number of three-mode grids drastically to only 10, and thus, the number of ab initio energies needed is on the order of 1000 for these grids.

To find the optimal electronic structure method that is both practical and relatively accurate, we tested a variety of size-extensive methods, including MP2, MP3, MP4, QCISD, CCSD, and (MR)ACPF, with triple- $\zeta$  quality basis sets. A simple estimate of the least number of single point energy calculations (without the gradient) needed to map out the 30-dimensional surface easily ruled out the much more expensive nonlinear, iterative methods, which can be used as a benchmark for testing the accuracy of perturbation theory and for addressing possible problems of apparent multireference character of the electronic wavefunction, that is, a superposition of the neutral and zwitterionic configurations in the presence of a polar solvent.<sup>15</sup> Since our goal is to create a realistic description of the potential surface, that is, to go beyond the minimal one- and two-mode representation, the method of choice appears to be MP2 with a suitably chosen correlation consistent basis set. Exploratory fine-tuning of the basis set versus computational time per calculation allowed us to add diffuse  $s$  and  $p$  functions to cc-pVTZ on O and N. This flexibility improves description of the long range interaction between O and the H atoms from the methyl groups, as well as adds diffuse orbital character needed for possible excess negative charge accumulation and charge fluctuation between O and N. This basis is referred to as aug-cc-pVTZ.

To construct the grids, we first optimized the geometry to the global minimum with very tight convergence criteria and performed a frequency calculation, that is, calculation and diagonalization of the second derivative matrix. We used Gaussian 98<sup>28</sup> with the semidirect option for MP2, to avoid memory problems, and with a numerical option for the frequency calculation, which avoided a direct construction of the Hessian by way of central-difference gradient differentiation with a 0.001 Å step. These precautions ensured a precisely orthogonal set of Hessian eigenvectors that also retained the  $C_s$  point group symmetry elements for all atoms. Such care for detail is usually unnecessary in a simple visual analysis normal mode calculation, but it is crucial in our case for the construction of an exact  $C_s$ -symmetry adapted vibrational Hamiltonian. The Cartesian normal mode eigenvectors,  $\{\bar{u}_a\}_i$ , for atoms  $a = 1, \dots, 12$  and vibrational modes  $i = 1, \dots, 30$  were then used to define Cartesian displacements for the atoms from the equilibrium geometry, for example,  $\Delta \bar{r}_{a,i} = m_a^{-1/2} Q_i \bar{u}_{a,i}$  where  $Q_i$  is the displacement along mode  $i$ , and  $m_a$  is mass of atom  $a$ . All subsequent single point energy calculations were done with MOLPRO 2006.1<sup>29</sup> using the integral direct MP2 program.<sup>30</sup>

Our usual strategy in quantum vibrational calculations is to first define the range for each vibrational mode, namely, to find  $\min [Q_i]$  and  $\max [Q_i]$ . These values are determined by applying an energy threshold  $E_{\text{th}}$ . In the present case, we use  $E_{\text{th}} = 35\,000 \text{ cm}^{-1}$ , common for all modes. We used a modest 10 grid points per mode, which resulted in  $\sim 200$  one-mode calculations, exploiting the  $C_s$  symmetry. Grids varied for two-mode scans

between 8 and 9, depending on the symmetry and the shape of the potential; thus, approximately  $9 \times 8 \times 30 \times 29/4 = 15\,660$  two-mode calculations were done. Selected three-mode potentials were generated on the same grids as the two-mode potentials, resulting in an additional 10 000 points. Overall, the computational effort can be roughly converted to a month of CPU time on a 10-processor cluster and assuming an average of 20 min per energy calculation for MP2/aug-cc-pVTZ for the two possible symmetries.

The one-, two-, and three-mode intrinsic potentials were then least-squares fit using a polynomial fitting basis of the form  $(\tanh(\gamma_i Q_i))^n$ , where  $\gamma_i \equiv 1/\max[|Q_i|]$ . Given the symmetry of NMA, which possesses a plane of reflection, the  $A''$  vibrational modes are defined on one-half of their range, and only the even polynomial powers are retained in the fits. It is further assumed that the gradient vanishes exactly at the equilibrium where the potential is also set to zero. The highest power for each potential was determined to minimize both the rms error and the number of terms itself, to keep the polynomial as low order as possible. This was achieved by setting a threshold such that the lowest order polynomial with the rms smaller than a preset threshold (we used  $1\text{ cm}^{-1}$ ) was selected as best fit. All the one-mode fits and most of the two-mode fits were well within the  $1\text{ cm}^{-1}$  rms threshold; however, several two- and three-mode fits had slightly larger rms errors, typically between 3 and  $5\text{ cm}^{-1}$ . Finally, the polynomial expansion coefficients  $a_n^{(i)}$ ,  $a_{n_p, n_q}^{(i,j)}$ , and  $a_{n_p, n_q, n_r}^{(i,j,k)}$ , along with the normal mode eigenvectors, harmonic frequencies, atomic masses, and the equilibrium geometry were used as input for MULTIMODE.

### 3. Calculation of Vibrational Energies and Comparison with Experiment

Vibrational energy levels are obtained as eigenvalues of the Watson Hamiltonian with the potential shown in eq 1; namely,

$$H_{\text{vib}} \Psi_n^{\text{CI}}(\mathbf{Q}) = E_n^{\text{CI}} \Psi_n^{\text{CI}}(\mathbf{Q}) \quad (2)$$

where  $n$  is the eigenvalue/eigenfunction index, and  $\mathbf{Q}$  is the 30-dimensional vector of normal coordinates. The eigenfunctions  $\Psi_n^{\text{CI}}$  are linear combinations of direct products of one-dimensional basis functions  $\chi_i(Q_i)$ , which are the solutions of the corresponding VSCF equations.<sup>18,19</sup> The one-dimensional basis is first made up of 7–9 harmonic oscillator functions, which are then contracted to 5–7 quadrature-optimized functions. These quadrature-optimized functions form the one-dimensional basis  $\{\chi_i\}$  for the VSCF calculation. The overall procedure is, thus, to first solve the coupled SCF equations, one for each normal coordinate until convergence of the lowest energy level is reached, and second, to construct a configuration interaction (CI) matrix using the orthogonal virtual basis of the VSCF Hamiltonian and diagonalize it, yielding the final results,  $\{E_n^{\text{CI}}, \Psi_n^{\text{CI}}\}$ . This approach is referred to as the vibrational CI.<sup>18,19</sup> The size of the CI calculation is substantially reduced compared to nonoptimized, direct harmonic basis calculation. In addition, the convergence of the fundamental excitations with respect to CI basis size is usually achieved with only a few quadrature-optimized basis functions per mode.

Visual inspection of the two lowest frequency modes revealed two quasi-free  $\text{CH}_3$  rotations: one rotor,  $Q_1$ , having a near-zero frequency ( $14\text{ cm}^{-1}$ ) and attached to the amide nitrogen, and the other,  $Q_2$ , with a  $50\text{ cm}^{-1}$  frequency located on the amide carbon. The small harmonic frequencies have little significance because the potential along these modes is expected

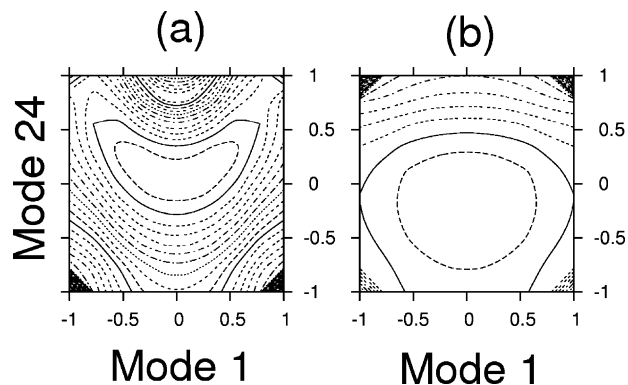


**Figure 1.** A contour plot of the potential along *N*-methyl rotation coordinate  $\gamma_1 Q_1$  (horizontal axis) and *N*-methyl breathing mode  $\gamma_{24} Q_{24}$  (vertical axis). The two plots illustrate the difference between the full potential (a) and the uncoupled potential (b).

to be dominated by the quartic powers. More importantly, these two torsional modes do mix with the associated symmetric CH stretches  $Q_{24}$  and  $Q_{25}$  because rectilinear normal modes are a poor description of curvilinear torsions. Although the barriers to both  $\text{CH}_3$  rotations are less than  $1\text{ kcal/mol}$ , the potentials in the  $(Q_1, Q_{24})$  and  $(Q_2, Q_{25})$  planes are very flat along the  $\text{CH}_3$  rotation coordinate. For an illustration, we refer to Figure 1. The location of the rotational transition state is correctly shown in either of the upper corners of the full potential in Figure 1a, but it is completely missing in the uncoupled potential in Figure 1b. The rigorous treatment of the large amplitude motion of the two methyl rotors is beyond the scope of a standard normal mode Hamiltonian, and we dealt with this, as usual, by not allowing high-energy excitations in these modes in the CI calculation. Specifically, the excitations in these and the next two lowest-frequency modes were restricted to a single quantum. (It is perhaps also worth noting that, in the present case, this approach is consistent with the expectation that in the condensed phase, the  $\text{CH}_3$  rotations are hindered due to their interactions with the solvent molecules.)

Results of the vibrational CI calculations, which are reported as energies relative to the zero point level, are summarized in Tables 1–3. The main bands of interest are the five  $A'$  modes (which we will refer to as the “amide modes”) that span the amide band region and that were the ones described in the recent work of Hayashi et al.<sup>15</sup> In our calculations, these are modes 12, 15, 22, 23, and 30. They describe the in-plane vibrations of the HNCO group and, thus, contain direct information about the dynamics of the peptide bond. So-called amide I, II, and III bands correspond to the fundamental of modes 23, 22, and 15, respectively. Figure 2 shows the normal mode vectors of these five modes.

We first examine convergence of these five band frequencies with respect to mode coupling (Table 1). This is useful for determining the importance of other modes, which we refer to loosely as the “bath modes”. The strictly harmonic frequencies are also included as a “baseline”. Consider first the uncoupled Hamiltonian but with the anharmonic terms included, that is, the 1MR level of theory. As seen, relative to the harmonic values, there are insignificant shifts in the first four fundamentals listed, but the NH stretch is red-shifted by  $136\text{ cm}^{-1}$ . Such a dramatic difference can be rationalized by analyzing the shapes of the potentials. The five one-mode potentials are shown in Figure 3. At low energies, up to  $5000\text{ cm}^{-1}$ , the NH stretch is already highly asymmetric, whereas the other four modes are dominated by the quadratic power. Inspection of the fitting coefficients confirms the visual analysis.

**TABLE 1: Convergence of the Amide-Band Fundamental Frequencies (in  $\text{cm}^{-1}$ ) for Various Levels of Mode Coupling in the Potential (as Described in the Text) Computed with MP2/aug-cc-pVTZ**

mode	character	H.O.	1MR <sup>a</sup>	2MR-A <sup>b</sup>	2MR-A2 <sup>b</sup>	2MR <sup>c</sup>	3MR-A <sup>d</sup>	exptl <sup>e</sup>
$\nu_{12}$	NH + CH <sub>3</sub> (N)	1119	1120	1122	1106	1103	1099	1089 <sup>f</sup>
$\nu_{15}$	NH + CH <sub>3</sub> (C)	1290	1296	1285	1258	1256	1253	1258
$\nu_{22}$	C–N	1561	1565	1555	1514	1516	1519	1500
$\nu_{23}$	C–O	1749	1743	1747	1726	1727	1727	1728
$\nu_{30}$	N–H	3703	3567	3552	3547	3531	3544	3498

<sup>a</sup> Size of CI matrix blocks: 118 ( $A'$ ) and 33 ( $A''$ ) <sup>b</sup> 711 and 331 <sup>c</sup> 777 and 355 <sup>d</sup> 791 and 331 <sup>e</sup> Experimental values are taken from ref 2. <sup>f</sup> Experimental value is taken from ref 1.

**TABLE 2: Fundamental Transition Frequencies for the ‘Bath’ Modes of NMA at 2MR Level of Theory**

mode	character	H.O.	2MR	exptl <sup>a</sup>	mode	character	H.O.	2MR	exptl <sup>a</sup>
$\nu_1(A'')$	CH <sub>3</sub> (N) rot.	0	438		$\nu_{16}(A')$	CH <sub>3</sub> (C) ubmr.	1402	1388	1370
$\nu_2(A'')$	CH <sub>3</sub> (C) rot.	50	375		$\nu_{17}(A')$	CH <sub>3</sub> (N) ubmr.	1460	1442	1419
$\nu_3(A'')$	C(+)-N(-)-C(+)	151	145		$\nu_{18}(A'')$	CH <sub>3</sub> (C) a-bend	1487	1467	1432
$\nu_4(A')$	CO rock	259	282	279	$\nu_{19}(A'')$	CH <sub>3</sub> (N) a-bend	1494	1483	1446
$\nu_5(A'')$	NH wag.	347	559		$\nu_{20}(A')$	CH <sub>3</sub> (C) s-bend	1498	1481	1446
$\nu_6(A')$	CO in-plane	423	438	439	$\nu_{21}(A')$	CH <sub>3</sub> (N) s-bend	1529	1505	1472
$\nu_7(A')$	CC str.	630	633	658	$\nu_{24}(A')$	CH <sub>3</sub> (N) brth.	3088	2940	2958
$\nu_8(A'')$	CO out-plane	633	685	626	$\nu_{25}(A')$	CH <sub>3</sub> (C) brth.	3091	2983	2915
$\nu_9(A')$	NCO bend	883	886	857	$\nu_{26}(A'')$	CH <sub>3</sub> (N) a-str.	3165	2995	2973
$\nu_{10}(A')$	CH <sub>3</sub> (C) rock	1003	1005	990	$\nu_{27}(A')$	CH <sub>3</sub> (C) a-str.	3188	3043	3008
$\nu_{11}(A'')$	CH <sub>3</sub> (C) twist	1058	1061	1037	$\nu_{28}(A'')$	CH <sub>3</sub> (C) a-str.	3188	3025	3008
$\nu_{13}(A'')$	CH <sub>3</sub> (N) twist	1169	1167		$\nu_{29}(A')$	CH <sub>3</sub> (N) a-str.	3197	3056	2978
$\nu_{14}(A')$	CH <sub>3</sub> (N) rock	1195	1199	1181					

<sup>a</sup> Experimental values are taken from ref 1.

**TABLE 3: Overtones and Combinations of NMA’s Amide Band ( $\text{cm}^{-1}$ )<sup>a</sup>**

state	H.O.	3MR-A	exptl <sup>b</sup>	state	H.O.	3MR-A	exptl <sup>b</sup>
$2\nu_{12}$	2238	2192		$3\nu_{12}$	3357	3282	
$\nu_{12} + \nu_{15}$	2409	2359		$2\nu_{23}$	3499	3433	3440
$2\nu_{15}$	2581	2503	2504	$\nu_{12} + 2\nu_{15}$	3700	3619	
$\nu_{12} + \nu_{22}$	2679	2626		$3\nu_{15}$	3871	3749	
$\nu_{15} + \nu_{22}$	2851	2773	2758	$\nu_{12} + \nu_{30}$	4816	4583	
$\nu_{12} + \nu_{23}$	2868	2837		$\nu_{15} + \nu_{30}$	4993	4738	
$\nu_{15} + \nu_{23}$	3040	2990	2971	$\nu_{22} + \nu_{30}$	5263	5006	
$2\nu_{22}$	3132	3030		$\nu_{23} + \nu_{30}$	5452	5209	
$\nu_{22} + \nu_{23}$	3310	3257		$2\nu_{30}$	7406	6871	

<sup>a</sup> The 3MR-A zero point level is  $22557 \text{ cm}^{-1}$ . <sup>b</sup> Experimental values are taken from ref 2.

Coupling the five modes among themselves with two-mode potentials while keeping all the other modes at 1MR level is the lowest order of amide mode correlation, referred to as 2MR-A. Overall, the corrections are small relative to the 1MR calculations. The effect of the bath modes is probed by coupling them to the amide modes via the two-mode amide-bath potentials (2MR-A2 level of theory); the bath modes are not coupled to each other in this representation. The coupling produces significant shifts relative to the 2MR-A results. The final 2MR calculation is where all modes are coupled at this level. As seen, there are only small shifts for relative to the 2MR-A2 ones, suggesting that the bath–bath coupling is not important for calculating the amide frequencies, at least at the 2MR level of theory. (A more complete set of 2MR results is shown in Table 2 and Figure 4.)

Finally, consider the effect of including three-mode coupling among the amide modes (3MR-A). With the exception of the NH stretch, the changes are small relative to the 2MR and 2MR-A2 calculations. Overall, the agreement with the available experimental data is remarkably good for the fundamental frequencies, and it is interesting and, we believe, significant that the level of agreement with experiment increases as the level of mode coupling increases. In addition, the rapid convergence of the amide band frequencies is an encouraging sign for applying the present formalism to generic system-bath

problems for which it may be desirable to treat a large number of bath modes explicitly at the quantum level.

Excitation energies of overtones and mode combinations are shown in Table 3. Wherever possible, comparison to experimental data is made. As is the case for the fundamental frequencies, the agreement with experiment is excellent, and in most instances, the frequency is overestimated rather than underestimated.

We constructed an approximate 0 K spectrum using the fundamental transition frequencies from the 3MR-A calculation and the intensities from the double harmonic MP2 calculation, that is, quadratic potential and linear dipole. To make a direct comparison with experiment,<sup>5</sup> the peaks were broadened using Gaussian functions with  $20 \text{ cm}^{-1}$  widths. The amide I, II, and III features can be easily identified around 1200–1300, 1400–1500, and 1700–1900  $\text{cm}^{-1}$  regions, shown in Figure 5. This calculated spectrum is in very good agreement with the one reported by Kubelka and Keiderling.<sup>5</sup> The increasing intensity of the amide bands with the frequency is reproduced well, and the region of weak absorption to the red of amide II is present in the calculated spectrum. The main discrepancy is the overestimated intensity for amide II, which is attributed to the double harmonic approximation used in the calculation. When the intensities of all peaks are scaled with the squared VCI coefficient of the leading configuration, which is  $\sim 0.92$  for amides II and III, and  $\sim 0.99$  for the other fundamentals, the spectrum is improved (the dashed line in Figure 5a). Further improvement can be achieved if the intensities are computed at the 2MR or 3MR-A level with an exact dipole. The other point of discrepancy is the doublet structure in amide I. Experimentally, the split is identified as being due to rotational transitions; namely, a B-type doublet, which could be significant at  $\sim 373 \text{ K}$ .<sup>5</sup> Since the calculated spectrum was done for a rotationless NMA at 0 K, the doublet structure is missing.

In the presence of solvent, the spectral features will shift, and the lines will broaden further due to solute–solvent interactions. This was discussed in detail by Hayashi et al.,<sup>15</sup> who predicted substantial shifts for amides I, II, and A on the

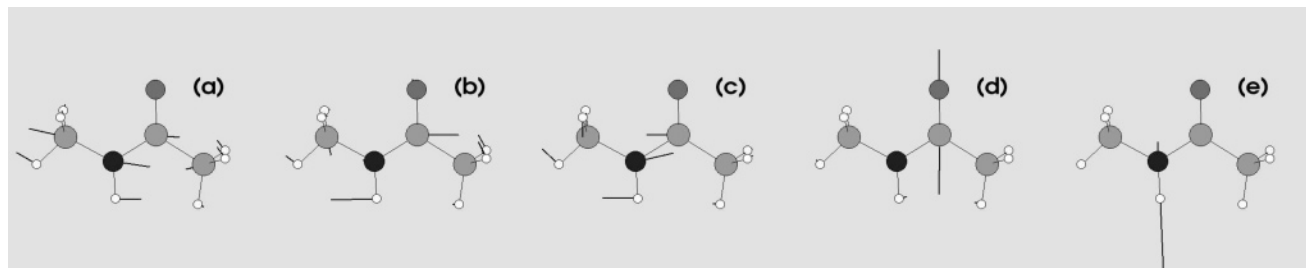


**Figure 2.** Normal coordinate definitions at MP2/aug-cc-pVTZ level for (a)  $Q_{12}$ , (b)  $Q_{15}$  amide III, (c)  $Q_{22}$  amide II, (d)  $Q_{23}$  amide I, and (e)  $Q_{30}$  amide A.

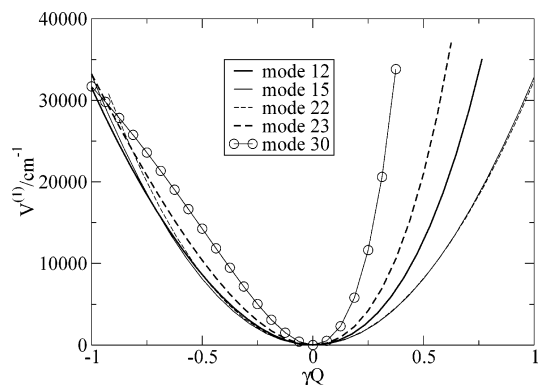


**Figure 3.** One-dimensional potentials,  $V^{(1)}$ , along the normal modes depicted in Figure 2. The values of  $\gamma$  are 0.0084, 0.010 95, 0.012 97, 0.011 16, and 0.016 24, in increasing frequency.

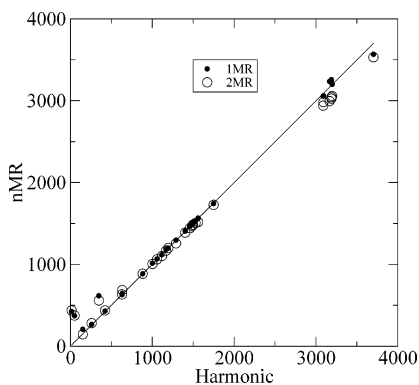


**Figure 4.** Correlation of the 1MR and 2MR frequencies of the fundamental transitions with the harmonic ones, in  $\text{cm}^{-1}$ .

basis of coupled quantum-classical simulations, consistent with the experiment. Similarly, *ab initio* MD calculations by Bour and Keiderling<sup>31</sup> showed big shifts of the amide frequencies in water.

#### 4. Summary and Future Work

We reported a calculation of vibrational energies of *N*-methyl acetamide using the code MULTIMODE, which makes use of  $n$ -mode representations of the potential in normal coordinates and with an exact vibrational Hamiltonian, inclusive of full vibration–rotation coupling. The potential was obtained as fits to electronic energies on the various  $n$ -mode grids, obtained with MP2 theory and a correlation consistent “pVTZ” basis set with the addition of diffuse  $s$  and  $p$  functions for O and N atoms. The focus of the calculations was on five modes that span the region of the amide bands. All 30 vibrational modes were considered; however, by using partitions of small groups of coupled modes, up to three for the five “amide” modes and only two for the other modes, we demonstrated good convergence of the vibrational energies of the amide modes. Agreement

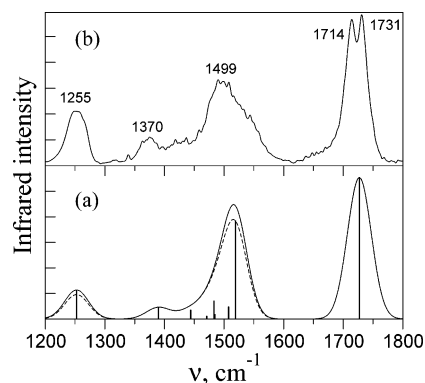


**Figure 5.** A comparison of (a) the calculated spectrum at 0 K with (b) the experimental one at  $\sim 373$  K provided by authors of ref 5. The number labels are the experimentally identified transitions in wavenumbers for the amides III (1255), II (1499), and I (1731). In the calculated spectrum, the stick positions are the 3MR-A frequencies from Table 1, and their height is the double harmonic calculation from MP2/aug-cc-pVTZ. The solid and the dashed lines are Gaussian convolutions of the sticks with a  $20 \text{ cm}^{-1}$  width. The dashed line was obtained from the sticks whose height was scaled by the leading VCI coefficient, squared, in the corresponding eigenstate (see text for explanation).

with experimental energies for the three amide bands was obtained with a very good level of accuracy, that is, a mean absolute deviation of  $16 \text{ cm}^{-1}$  for 3MR-A, as compared to a mean absolute deviation  $70 \text{ cm}^{-1}$  for the harmonic approximation. The infrared spectrum was also calculated and compared to experiment, where again, very good agreement was found.

The present calculations showed rapid convergence at a fairly low level of mode-coupling among the amide modes and an even lower level of coupling for the remaining 15 “bath modes”. This is encouraging for further studies that are planned to include explicit microsolvation.

As was suggested in previous studies,<sup>4,15</sup> the energies and wave functions for a microsolvated system can be calculated. The NMA–water interactions can be modeled reasonably well by force fields, as has been done recently.<sup>12,15,31</sup> Finally, the orthogonal states  $\{\Psi_n^{\text{CI}}\}$  can serve as a basis for expansion of a wavepacket evolving in time. We note that similar calculations are being done by other groups.<sup>34</sup> This is a subject of ongoing work that will be presented in a future publication.

**Acknowledgment.** We thank Dr. J. Kubelka and T. Keiderling for providing their experimental data. J.M.B. thanks the National Science Foundation (CHE-0446527) for financial support.

#### References and Notes

- (1) Ataka, S.; Takeuchi, H.; Tasumi, M. *J. Mol. Struct.* **1984**, *113*, 147.
- (2) Mayne, L. C.; Hudson, B. *J. Phys. Chem.* **1991**, *95*, 2962.

- (3) Chen, X. G.; Schweitzerstener, R.; Asher, S. A.; Mirkin, N. G.; Krimms, S. *J. Phys. Chem.* **1995**, *99*, 3074.
- (4) Torii, H.; Tasumi, T.; Tasumi, M. *J. Raman Spectrosc.* **1998**, *29*, 537.
- (5) Kubelka, J.; Keiderling, T. A. *J. Phys. Chem. A* **2001**, *105*, 10922.
- (6) Cuevas, G.; Renugopalakrishnan, V.; Madrid, G.; Hagler, A. T. *Phys. Chem. Chem. Phys.* **2002**, *4*, 1490.
- (7) Papamokos, G. V.; Demetropoulos, I. N. *J. Phys. Chem. A* **2004**, *108*, 7291.
- (8) Zhang, R.; Li, H. R.; Lei, Y.; Han, S. J. *J. Mol. Struct.* **2004**, *693*, 17.
- (9) Mirkin, N. G.; Krimm, S. *J. Am. Chem. Soc.* **1991**, *113*, 9742.
- (10) Gregurik, S. K.; Chaban, G. M.; Gerber, R. B. *J. Phys. Chem. A* **2002**, *106*, 8696.
- (11) Weiner, S. J.; Kollman, P. A.; Case, D. A.; Singh, U. C.; Ghio, C.; Alagona, G.; Profeta, S., Jr.; Weiner, P. *J. Am. Chem. Soc.* **1984**, *106*, 765.
- (12) Iuchi, S.; Morita, A.; Kato, S. *J. Phys. Chem. B* **2002**, *106*, 3466.
- (13) Gaigeot, M. P.; Vuilleumier, R.; Sprik, M.; Borgis, D. *J. Chem. Theory Comput.* **2005**, *1*, 772.
- (14) Mantz, Y. A.; Gerard, H.; Iftimie, R.; Martyna, G. J. *J. Am. Chem. Soc.* **2004**, *126*, 4080.
- (15) Hayashi, T.; Zhuang, W.; Mukamel, S. *J. Phys. Chem. A* **2005**, *109*, 9747.
- (16) Car, R.; Parrinello, M. *Phys. Rev. Lett.* **1985**, *55*, 2471.
- (17) MULTIMODE is a variational code for the calculation of rovibrational energies of large polyatomic molecules; written by S. Carter, with contributions from B. J. Braams, J. M. Bowman, and N. C. Handy.
- (18) Carter, S.; Culik, S. J.; Bowman, J. M. *J. Chem. Phys.* **1997**, *107*, 10458.
- (19) Carter, S.; Bowman, J. M.; Handy, N. *Theor. Chem. Acc.* **1998**, *100*, 191.
- (20) Watson, J. K. G. *Mol. Phys.* **1968**, *15*, 479.
- (21) Bowman, J. M.; Carter, S.; Huang, X. *Int. Rev. Phys. Chem.* **2003**, *22*, 533.
- (22) Bowman, J. M.; Carter, S.; Handy, N. C. In *Theory and Applications of Computational Chemistry: The First 40 Years*; Dykstra, C., Frenking, G., Kim, K. S., Scuseria, G. E., Eds.; Elsevier: Amsterdam, 2005; Chapter 11.
- (23) Wu, J.; Huang, X.; Carter, S.; Bowman, J. M. *Chem. Phys. Lett.* **2006**, *426*, 285.
- (24) Irlle, S.; Bowman, J. M. *J. Chem. Phys.* **2000**, *113*, 8401.
- (25) Yagi, K.; Taketsugu, T.; Hirao, K.; Gordon, M. S. *J. Chem. Phys.* **2000**, *113*, 1005.
- (26) Rauhut, G. *J. Chem. Phys.* **2004**, *121*, 9313.
- (27) Gerber, R. B.; Chaban, G. M.; Brauer, B.; Miller, Y. In *Theory and Applications of Computational Chemistry: The First 40 Years*; Dykstra, C., Frenking, G., Kim, K. S., Scuseria, G. E., Eds.; Elsevier: Amsterdam, 2005; Chap. 9.
- (28) Frisch, M. J.; Trucks, G. W.; Schlegel, H. B.; Scuseria, G. E.; Robb, M. A.; Cheeseman, J. R.; Zakrzewski, V. G.; Montgomery, J. A., Jr.; Stratmann, R. E.; Burant, J. C.; Dapprich, S.; Millam, J. M.; Daniels, A. D.; Kudin, K. N.; Strain, M. C.; Farkas, O.; Tomasi, J.; Barone, V.; Cossi, M.; Cammi, R.; Mennucci, B.; Pomelli, C.; Adamo, C.; Clifford, S.; Ochterski, J.; Petersson, G. A.; Ayala, P. Y.; Cui, Q.; Morokuma, K.; Malick, D. K.; Rabuck, A. D.; Raghavachari, K.; Foresman, J. B.; Cioslowski, J.; Ortiz, J. V.; Stefanov, B. B.; Liu, G.; Liashenko, A.; Piskorz, P.; Komaromi, I.; Gomperts, R.; Martin, R. L.; Fox, D. J.; Keith, T.; Al-Laham, M. A.; Peng, C. Y.; Nanayakkara, A.; Gonzalez, C.; Challacombe, M.; Gill, P. M. W.; Johnson, B. G.; Chen, W.; Wong, M. W.; Andres, J. L.; Head-Gordon, M.; Replogle, E. S.; Pople, J. A. Gaussian 98, revision A.11.4; Gaussian, Inc.: Pittsburgh, PA, 1998.
- (29) H.-J. Werner, P. J. Knowles, R. Lindh, F. R. Manby, M. Schütz, and others, MOLPRO, version 2006.1, a package of ab initio programs; <http://www.molpro.net>.
- (30) Schütz, M.; Lindh, R.; Werner, H.-J. *Mol. Phys.* **1999**, *96*, 719.
- (31) Bour, P.; Keiderling, T. A. *J. Chem. Phys.* **2003**, *119*, 11253.
- (32) Hetzer, G.; Schütz, M.; Stoll, H.; Werner, H.-J. *J. Chem. Phys.* **2000**, *113*, 9443.
- (33) Weigend, F.; Haser, M.; Patzelt, H.; Ahlrichs, R. *Chem. Phys. Lett.* **1998**, *294*, 143.
- (34) Fujisaki, H.; Yagi, K.; Hirao, K.; Straub, J. E. Unpublished results.